Postprint version of the paper published in J.Therm.Anal.Calorim. (2016) 125:571–577

Measuring thermal conductivity of powders with differential scanning calorimetry: a simplified method

Pujula, Miquel[1]; Sánchez-Rodríguez, Daniel[1]; Lopez-Olmedo, Joan Pere[2]; Farjas, Jordi[1]; Roura, Pere[1]*

[1]GRMT, Department of Physics, University of Girona, E17071-Girona, Catalonia (Spain)

[2]Unitat d'Anàlisi Tèrmica (STR), University of Girona, E17071Girona, Catalonia (Spain)

*corresponding author: pere.roura@udg.cat, Tel. 34972418383 Fax. 34972418098

Keywords: thermal conductivity, powders, DSC, alumina

Abstract

This paper simplifies a recently proposed method for measuring the thermal conductivity of powders using Differential Scanning Calorimetry (DSC) [D. Sánchez-Rodríguez, J. P. López-Olmedo, J. Farjas and P. Roura., Determination of thermal conductivity of powders in different atmospheres by differential scanning calorimetry. J. Therm. Anal. Calorim. 2015; 121:469–473][1]. With this method a crucible is filled with powder and a spherical metal reference is partially sunk into it. The thermal resistance between the metal and the crucible wall at the metal melting point is obtained from the DSC melting peak slope. In the simplified method outlined this paper, a cylindrical pan is substituted for the original hemispherical crucible. The equivalence of both methods is demonstrated with alumina powder and commercial cylindrical crucibles of several sizes and aspect ratios.

1.- Introduction

The thermal conductivity of powders is much lower (10-100 times) than that of their bulk counterparts [2, 3]. For relative densities below 80% and small particle sizes (< 100 μm) heat-flow is governed by interparticle contact resistance [4]. This surprising behaviour renders metallic powders as insulating as ceramic powders [5, 1] and has significant consequences for the combustion synthesis of materials [3, 6, 7, 8] and for thermal insulation [9]. As such, the low thermal conductivity of powders reduces DSC analysis accuracy as a result of the thermal gradients that develop inside the sample [10]. It can be obtained by measuring the thermal resistance of a powder filling the volume between a hot wire and a concentric cylinder [2, 9] or, alternatively, it can be measured by the transient hot source method, which applies a constant heat power [11], or by the 3ω method based on harmonics detection [12].

That said, we have recently demonstrated that the thermal conductivity of powders can also be measured by Differential Scanning Calorimetry (DSC) [1]. Our method is an adaptation of Camirand's method [13] that relies on the analysis of the low-temperature side of the melting peak of selected metals. From its slope (Fig.1), the thermal resistance, R (Fig.1 – R_{DSC} is the sensor's thermal resistance), of the powder sample is deduced and its thermal conductivity, κ, extracted. Hemispherical aluminium pans were made to hold the powder and to simplify the analysis (Fig.2a). For this particular geometry, the relationship between κ and R is easily calculated:

$$R_h = \frac{1}{\pi\kappa}\left(\frac{1}{D_m} - \frac{1}{D_p}\right), \qquad (1)$$

where D_p and D_m are the diameters of the pan and the metal reference bead, respectively, and subscript h stands for "hemispherical". The main disadvantage of this method is the need for a non-commercial hemispherical crucible.

The present study is devoted to showing that cylindrical crucibles can be used instead (Fig.2b). First of all (Section 2), we will demonstrate that for any crucible geometry, and after a transient period, the slope of the melting peak continues to be $1/(R+R_{DSC})$. The problem is thus reduced to generalizing eq.(1) for cylindrical geometry. A finite element code has been developed in Section 3 to discern the dependence of R on geometry (D_m, D_p and the pan height, H). The results can be summarized with the ratio, K, between the actual resistance, R, and that of a hemispherical crucible with the same diameter:

$$K \equiv \frac{R}{R_h}. \qquad (2)$$

Once tabulated, this parameter can be used to obtain the thermal conductivity of powders from R. This new method has been validated by measuring the thermal conductivity of alumina powder with several commercial crucibles (Section 4). The paper concludes with a brief summary.

2.-Theoretical development

a) Isothermal and isochronal surfaces

During a standard DSC experiment, the furnace temperature, T_f, is raised at a constant rate,

$$dT_f/dt = \beta. \qquad (3)$$

The temperature distribution in the powder, which is filling the volume between the pan and the metal reference bead (Fig.2b), will obey the heat transport equation:

$$\kappa\Delta T + \overrightarrow{div}\kappa \cdot \vec{\nabla}T = \rho c \frac{\partial T}{\partial t}, \qquad (4)$$

(ρ and c are the powder mass density and specific heat capacity, respectively), and will reach two asymptotic solutions depending on the metal temperature.

After an initial transient period, and before the reference metal begins to melt (the metal temperature, T_m, below its melting point, T_{MP}), pan, powder and reference metal will acquire the heating rate β. We have recently shown [10] that the temperature at any point in the powder will follow the programmed temperature with a time delay of $\tau(\vec{r})$ with respect to the pan temperature:

$$T(\vec{r}, t) - T_p(t) = \beta(t - \tau(\vec{r})). \qquad (5)$$

where $\tau(\vec{r})$ is time-independent provided that no thermal losses occur at the external top surfaces and that the material's parameters (κ, ρ, c) are temperature-independent [10]. Under these conditions, the isothermal surfaces are those of constant τ. Their shape depends on κ and ρc, and is independent of β.

Once the reference metal reaches its melting point, its surface will remain at T_{MP} during the melting process. Consequently, the boundary conditions for the powder will now be: (i) constant temperature rise next to the crucible walls and (ii) constant temperature next to the metal. In the Supporting Information File, we demonstrate that the asymptotic solution consists of a series of isochronal surfaces (i.e. surfaces where dT/dt = constant).

The nice result is that these isochronal surfaces match the isothermal surfaces of the steady-state solution (Fig. 3), i.e. the temperature distribution when the temperature is held constant at both the metal reference bead and pan surface. For a homogeneous powder, their shape depends exclusively on the geometry of the pan and the reference metal. For an inhomogeneous powder it will also depend on the spatial variation of κ.

The evolution from isothermal to isochronal surfaces does not occur abruptly as soon as melting begins, but rather requires a transient period.

b) Slope of the DSC melting peak

In the Supporting Information File, we show that, after this transient period, the pan temperature, T_p, reaches a constant heating rate equal to:

$$\beta_p = \frac{R}{R_{DSC}+R}\beta. \quad (6)$$

Since the DSC Reference temperature follows the furnace temperature,

$$dT_{REF}/dt = \beta, \quad (7)$$

we deduce that the DSC signal:

$$\dot{Q}_{DSC} = \frac{T_p - T_{REF}}{R_{DSC}} \quad (8)$$

will grow linearly with time:

$$\frac{d\,\dot{Q}_{DSC}}{dt} = -\frac{\beta}{R_{DSC}+R} \quad (9)$$

and, consequently, the slope of the DSC curve will be equal to:

$$\frac{d\dot{Q}_{DSC}}{dT_{REF}} = \frac{-1}{R_{DSC}+R} \quad . \quad (10)$$

Notice that the results of this section are independent of the pan and reference metal shapes. They are valid if the powder free surface is adiabatic. According to eq.(10), the powder resistance can be obtained from the slope of the DSC peak measured with the powder ($1/R_{DSC}+R$) and of that measured without it ($1/R_{DSC}$).

c) The transient period

Experimental determination of R is only possible if the asymptotic state of the isochronal surfaces has been reached after a transient period, which begins with the onset of melting. Here, we simply want to analyze what experimental conditions make it easier to reach this asymptotic state. This state will be reached if the duration of the transient period, Δt_{trans}, is shorter than the amount of time needed for the reference metal to melt, Δt_m, i.e.:

$$\Delta t_{trans} < \Delta t_m \, . \quad (11)$$

When the boundary condition at the reference metal is suddenly changed from $\beta \neq 0$ to $\beta = 0$, the evolution time from one to the other asymptotic solutions (Figs.3a and 3b) of the heat transport equation (eq.(4)) will be proportional to the inverse of the powder thermal diffusivity ($\kappa/\rho c$), i.e.:

$$\Delta t_{trans} = C\,\frac{\rho c}{\kappa} \, , \quad (12)$$

where constant C depends, in a non-trivial way, on the geometry of the system and is roughly proportional to the "thickness" of the powder squared $[(D_p-D_m)^2]$[14].

For Δt_m, heat flows to the metal reference at the rate

$$\dot{Q}_m = \frac{T_p - T_m}{R} \cong \frac{\beta t}{R} \ , \qquad (13)$$

where the last term holds because $T_p \approx T_m$ at the onset of melting and $\beta_p \approx \beta$ for the usual situation of $R >> R_{DSC}$ (eq.(6)). Integration of eq.(13) from t = 0 to Δt_m must be equal to the heat of fusion $l_F \cdot m$ of the reference metal of mass m, and leads to the value

$$\Delta t_m = \sqrt{\frac{\pi}{3}\frac{R l_F \rho_m D_m^3}{\beta}} = G\sqrt{\frac{l_F \rho_m}{\beta \kappa}} \ , \qquad (14)$$

where ρ_m is the density of the metal and G is a geometrical factor.

In view of eqs.(12) and (14), we conclude that the asymptotic state for determining thermal resistance will be reached more easily when [eq.(11)]: a) powders have a higher thermal conductivity and a lower heat capacity per unit volume (ρc), b) the reference metal has a higher density and latent heat of fusion, and c) experiments are performed at a lower heating rate.

d) Powder thermal resistance

A finite element code has been developed to numerically solve the heat transport equation (eq.(4)) for a homogeneous powder (constant κ) under steady-state conditions. Since thermal resistance scales with linear size, R has been computed for a range of D_m/D_p and H/D_p (Fig.2b) values that cover virtually all commercial DSC cylindrical crucibles. The results are summarized in terms of parameter K (eq.(2)) in Fig.4. Each curve corresponds to crucibles with the same metal reference diameter (constant D_m/D_p)., For short crucibles ($H/D_p < 0.42$ approx.) we observe that resistance is lower ($K < 1$) for the cylindrical crucible than for the reference hemispherical crucible, while the contrary holds for tall crucibles. For $H/D_p > 1$, an asymptotic value is reached, which increases for larger metal references. Furthermore, notice that for those crucibles where $H/D_p \approx 0.42$, $1 < K < 1.03$, i.e. R takes a value near that of the crucible that circumscribes a hemisphere ($H/D_p = 0.5$), the departure of R from its value in the hemispherical crucible is negligible.

e) Crucible finite thermal resistance

Up until now, we have supposed that the pan behaves like a perfect conductor. However, in view that DSC crucibles have thin walls, one may wonder if the hypothesis of an isothermal pan surface is accurate enough, especially for the lateral walls. In the Supporting Information File, we show that for a pan close to $H/D_p = 0.5$, the temperature difference from the top to the bottom of the walls, ΔT, relative to T_p-T_m is in the steady-state:

$$\frac{\Delta T}{T_p - T_m} \cong \frac{1}{6d\left(\frac{1}{D_m} - \frac{1}{D_p}\right)}\frac{\kappa}{\kappa_p} \ , \qquad (15)$$

where d is the wall thickness and κ_p is the pan material conductivity. For shorter (taller) crucibles, ΔT will be smaller (higher) than in eq.(15). Thanks to the fact that powders have very small conductivities when compared with bulk materials [1, 2, 5], temperature gradients in the pan walls can be neglected. This situation holds, in particular, for the experiments we have done. Consequently, we can conclude that, in general, the thermal resistance measured will indeed correspond to that of the powder.

3.-Experimental details

The method has been tested with a Mettler Toledo heat flux DSC 822 on alumina powder (purity above 99%, 50-200 µm particle size [1]). We have used high purity In beads as the reference metal (ρ_m = 7.31 g cm^{-3}, l_F = 28.42 J g^{-1}, T_{MP} = 156.6ºC). Its mass was used to calculate the bead diameter (D_m) that varied from 1.2 to 2.7 mm. Several alumina, aluminum and platinum pans were used and their geometry and thermal properties are detailed in Table I.

The pans were completely filled with alumina powder and were gently tapped. At this point, powder relative density was measured and found to vary between 24% and 27%, except in the case of the tallest pan (pan A, Table I) where it was 19%. Afterwards, an In bed was sunk at the center of the powder surface, as shown in Fig.2a. DSC curves were usually recorded at 10 ºC min^{-1} in N_2 but, eventually, different heating rates were used. In some instances, lower heating rates were required to reach a constant slope during melting (see next section). For each pan we also measured the melting peak of an In sample flattened on the bottom of the crucible. This complementary experiment allowed us to determine the sensitivity of the apparatus which varied by up to 20% among the crucibles we used. In each and every one of the experiments, the first heating ramp was simply used to allow the metal bead to achieve good thermal contact with the powder or the pan and was not analyzed.

The slope of the baseline on the low-temperature side was subtracted to that of the melting peak. Without powder, experiments delivered slope values that varied within the 30-80 mW ºC^{-1} range revealing a non-negligible contribution of contact resistance, R_c, between the pan and the DSC sensor disc. In this case, the analysis given above continues to be valid when substituting R_{DSC} with $R_{DSC}+R_c$ [1].

4.-Results and discussion

In a first series of experiments we measured R with the alumina powder inside a 70 µL alumina pan (pan A in Table I). Several In metal reference beads with diameters in the 1.2-2.7 mm range were used. The values of R vs D_m have been plotted in Fig.5a. Notice that, as expected from eq.(1),

thermal resistance increases when D_m diminishes and varies by a factor of 3 along the whole range. On the other hand, for these particular experiments, K ranges from 1.04 to 1.14. Applying eqs.(1) and (2) delivers the powder thermal conductivity (Fig.5b). The low value of κ obtained for the smallest bead could be slightly under-evaluated because, for this particular experiment, melting occurs during the transient period (section 2c). In fact, if we plot the derivative of the melting peak of this small bead measured at 10 ºC min^{-1} (Fig.6), we see that a constant value is not reached. This is in contrast to the experiments done with the larger beads (dotted curve in Fig.6).

For this reason, we ran a second series of experiments with the same bead (D_m = 1.29 mm) but at different heating rates (5ºC, 10ºC, 20ºC and 40ºC min^{-1}). As expected from the analysis carried out in Section 2c, the slope increases for lower heating rates and, at 5ºC min^{-1}, a stable slope is almost reached (Fig.6). The corresponding values of the "apparent" conductivity are plotted in Fig.5b. If we take the point measured at 5ºC min^{-1}, we conclude that κ of the alumina powder is in the 0.117-0.129 W m^{-1} K^{-1} range.

In a third series of experiments, we used a single 2.26 mm diameter metal bead with all the crucibles listed in Table I. The results have been plotted in Fig.7 as κ vs R. Notice that, with the exception of pan C, the values of κ vary in a range (0.104-0.124 W m^{-1} K^{-1}) covering that which was obtained in the previous experiments, although with greater uncertainty. In the present series, melting persists long enough to reach a stable slope after the initial transient period. Even though pan B powder relative density (19.1 g cm^{-3}) was substantially smaller than that of the other pans (25-27 g cm^{-3}), we measured the same κ. This is not surprising, because κ varies very slowly at low relative density [16, 3]. The large deviation of pan C is due to the large experimental uncertainty related to the very small 0.3 mm gap between the bead and the crucible bottom (Fig.7). Consequently, this experiment has been discarded.

The results reported above compare favorably with the values of κ obtained with the hemispherical pan and two metal bead diameters (2.25 and 1.79 mm): 0.113 and 0.125 W m^{-1} K^{-1} (respectively). So, we can conclude that, within experimental accuracy, cylindrical and hemispherical pans deliver the same value of κ.

Before leaving this section, we would like to discuss two additional points: pan thermal resistance and heat losses. The application of eq.(15) to all the experiments delivers $|\Delta T|/T_p - T_m < 10^{-2}$. This means that the pan surface can be considered isothermal with very good approximation. In other words, pan thermal resistance can be neglected. As for heat losses, they can be easily quantified because the peak area was usually smaller with powder than without it. Fig.8 tells us that heat losses can be as high as 30%. Most of these losses occur at the metal bead's free

surface. This phenomenon has a null effect on the metal temperature during melting and, consequently, on determining the melting peak slope. If the thermal losses had occurred on the powder free surface, they could have had an effect on the peak slope. This effect cannot be discarded, but its analysis is outside the scope of the present work.

5.-Summary and conclusion

The possibility of measuring the thermal conductivity, κ, of powders from the slope of the melting peak of a pure reference metal has been demonstrated from a theoretical point of view. After a transient period, the slope reaches a constant value that is exactly the reciprocal of the powder resistance, R, plus the DSC sensor resistance. This result is valid for arbitrary pan geometry and, in particular, for standard cylindrical pans. To extract κ from R, it has been shown that for most commercial crucibles the powder resistance can be referred to that of a hemispherical pan corrected by a factor, K. The values of K have been calculated and, for most practical situations, they are close to 1. Experiments carried out on alumina powder have shown that its thermal conductivity can be measured within an error bar of ±10%. This accuracy is reached despite large amounts of heat escaping from the DSC sensor. In principle, since during solidification the temperature of metal beads remains constant and equal to the melting point, the method developed here can be used for measuring the thermal conductivity of powders during cooling ramps.

Our present study improves the method introduced in ref. [1] because it allows the use of commercial cylindrical crucibles and because it clearly shows that measurements are erroneous unless the constant slope of the melting peak is reached.

Acknowledgments

This work was partially funded by the Spanish Programa Nacional de Materiales through project MAT2014-51778-C2-2-R. The authors wish to thank the University of Girona for the PhD fellowship granted to Daniel Sánchez-Rodríguez and for the use of the thermal analysis facilities (Serveis Tècnics de Recerca).

References

[1] D.Sánchez-Rodríguez, J.P.López-Olmedo, J.Farjas, P.Roura, Determination of thermal conductivity of powders in different atmospheres by differential scanning calorimetry. J. Therm. Anal. Calorim. **121** (2015) 469–473.

[2] Z. Klemensiewicz, Thermal Conductivity of Powders, Nature, **164** (1949) 589-589.

[3] A.S. Mukasyan and A.S. Rogachev, Discrete reaction waves: gasless combustion of solid powder mixtures. Prog. Energy Combust. Sci. **34** (2008) 377-416.

[4] N.S. Goel, J.S. Geroc and G.A. Lehman, Simple model for heat conduction in heterogeneous materials and irregular boundaries. Int.Comm.Heat Mass Trans. **19** (1992) 519-530.

[5] A.V. Luikov, A.G. Shashkov, L.L. Vasiliev and Y.E. Fraiman, Thermal conductivity of porous media, Int.J.Heat.Mass Trans. **11** (1968) 117-140.

[6] A.P. Hardt and P.V. Phung, Propagation of gasless reactions in solids 1. Analytical study of exothermic intermetallic reaction rates. Combust. Flame **21** (1973) 77-89.

[7] D. Sanchez-Rodriguez, H. Wada, S. Yamaguchi, J. Farjas and H. Yahiro, Self-propagating high-temperature synthesis of LaMO3 perovskite-type oxide using heteronuclearcyano metal complex precursors. J.Alloys Comp. **649** (2015) 1291-1299

[8] P. Roura, J. Farjas, H. Eloussifi, L. Carreras, S. Ricart, T. Puig and X. Obradors, Thermochim. Acta **601** (2015) 1-8.

[9] L. Huang and M. S. El-Genk, Thermal conductivity measurements of alumina powders and molded Min-K in vacuum. Energy Convers.Manage. **42** (2001) 599-612.

[10] D.Sanchez-Rodriguez, H.Eloussifi, J.Farjas, P.Roura and M.Dammak , Thermal gradients in thermal analysis experiments: criterions to prevent inaccuracies when determining sample temperature and kinetic parameters, Thermochim. Acta **589** (2014) 37-46.

[11] L. Kubicar, V. Vretenar, V. Stofanik and V. Bohac, Hot-ball method for measuring thermal conductivity. Int.J.Thermophys. **31** (2010) 1904–1918.

[12] X. Zheng, L. Qiu, G. Su, D. Tang, Y. Liao and Y. Chen, Thermal conductivity and thermal diffusivity of SiO_2 nanopowder. J.Nanopart.Res. **13** (2011) 6887–6893.

[13] C.P.Camirand Measurement of thermal conductivity by differential scanning calorimetry. Thermochim Acta **417** (2004) 1–4.

[14] J.R.Welty, C.E.Wicks and R.E.Wilson(1984). Fundamentals of Momentum, Heat and Mass Transfer (New York: Wiley) Ch. 18.

[15] Y. Ming, J. Purewal, D. Liu, A. Sudik, C. Xu, J. Yang, M. Veenstra, K. Rhodes, R. Soltis, J. Warner, M. Gaab, U. Müller and D.J. Siegel, Thermophysical properties of MOF-5 powders, Microporous Mesoporous Mater. **185** (2014) 235-244.

[16] B.L. Huang, Z. Ni, A. Millward, A.J.H. McGaughey, C. Uher, M. Kaviany and O. Yaghi, Thermal conductivity of a metal-organic framework (MOF-5): Part II. Measurement, Int. J. Heat.Mass.Transfer, **50** (2007) 405-411.

Table I.- Geometry of pans (see Fig.2) and their thermal conductivity, κ_p

Pan	**Material**	**κ_p (W m^{-1} K^{-1})**	**d (mm)**	**H_p (mm)**	**D_p (mm)**	**H_p/D_p**
A	Alumina	30	0.5	4.05	4.95	0.82
B				3.89	8.04	0.48
C	Aluminum	230	0.22	1.46	5.4	0.27
D				5.8	5.6	1.04
E	Platinum	72	0.14	2.30	5.64	0.41
F				4.05	5.64	0.72
G	Aluminum	hemispherical			5.0	---

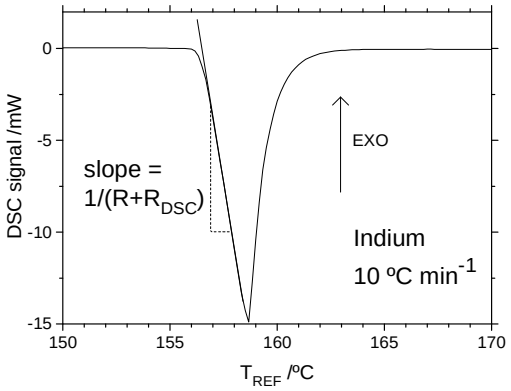

Figure 1.- The slope of the low-temperature side of the melting peak of a pure metal is related to the thermal resistance of the powder, R, and the DSC sensor resistance, R_{DSC} that is measured without powder (see main text).

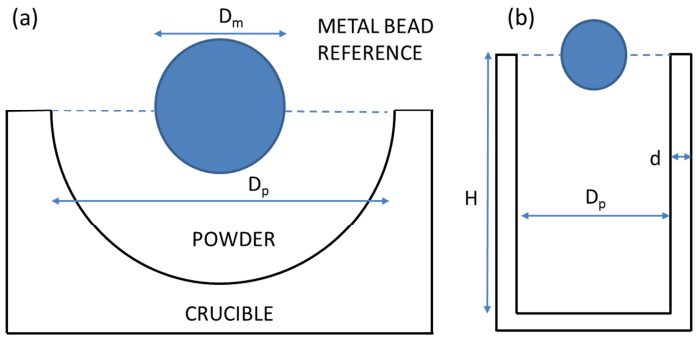

Figure 2.- Hemispherical crucible used previously [1] and the cylindrical crucibles used in the present work.

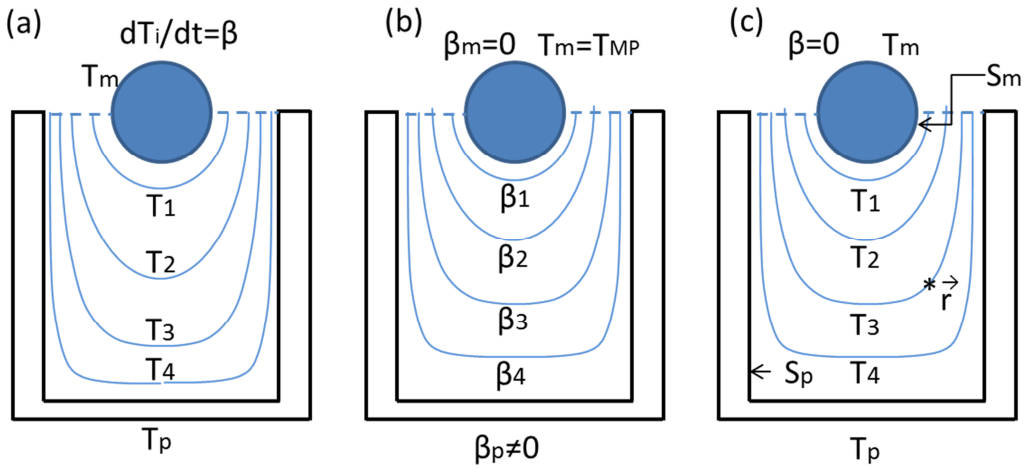

Figure 3.- Sketch of the isothermal and isochronal surfaces when the pan is heated at a constant heating rate: (a) before melting and (b) during melting. The isochronal surfaces of (b) coincide with the isothermal surfaces at the steady-state (c).

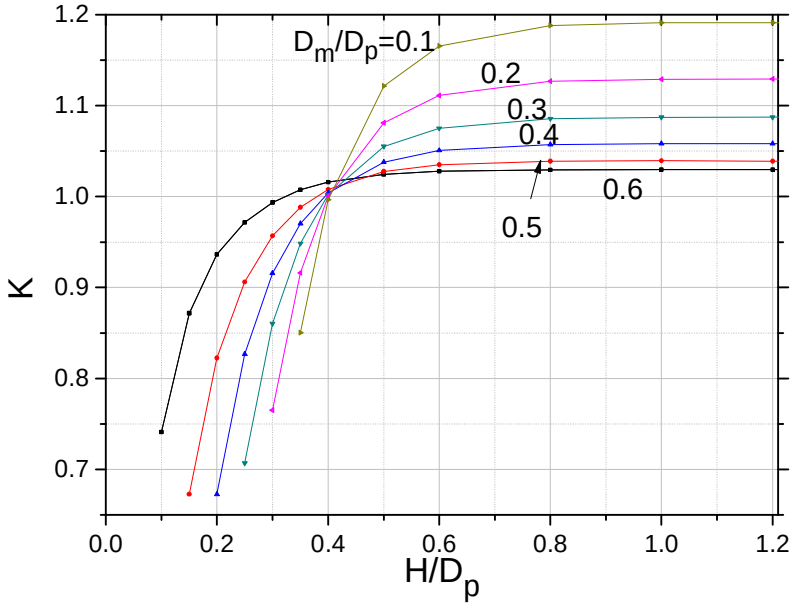

Figure 4.- Correction factor K as a function of the crucible height for several reference metal diameters.

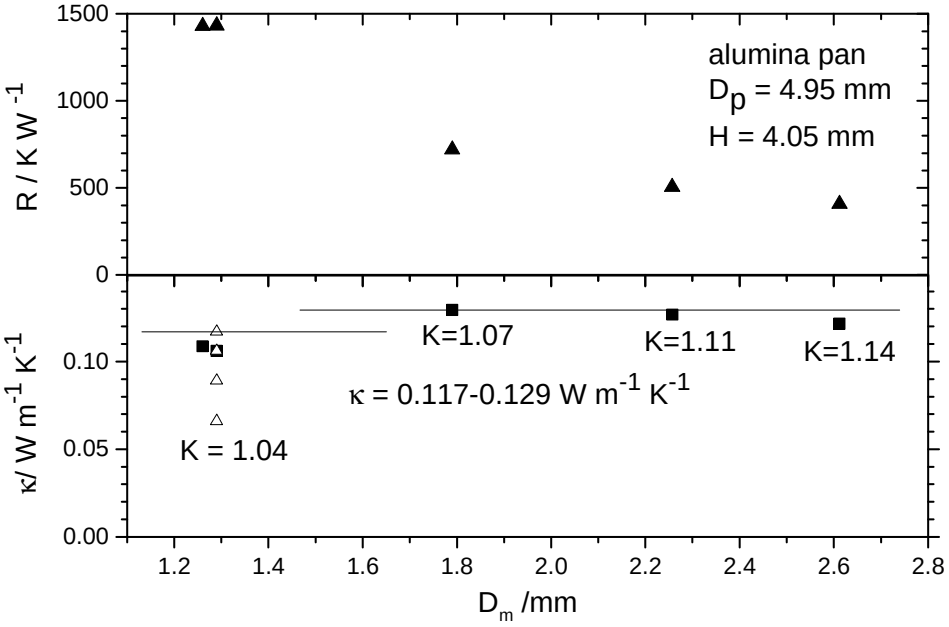

Figure 5.- a) Thermal resistance of the alumina powder contained between an alumina pan and a reference metal bead as a function of the bead diameter. b) Thermal conductivity of the powder. Open triangles correspond to the result obtained for varying heating rates (2, 5, 10 and 20 ºC min^{-1}, from top to bottom).

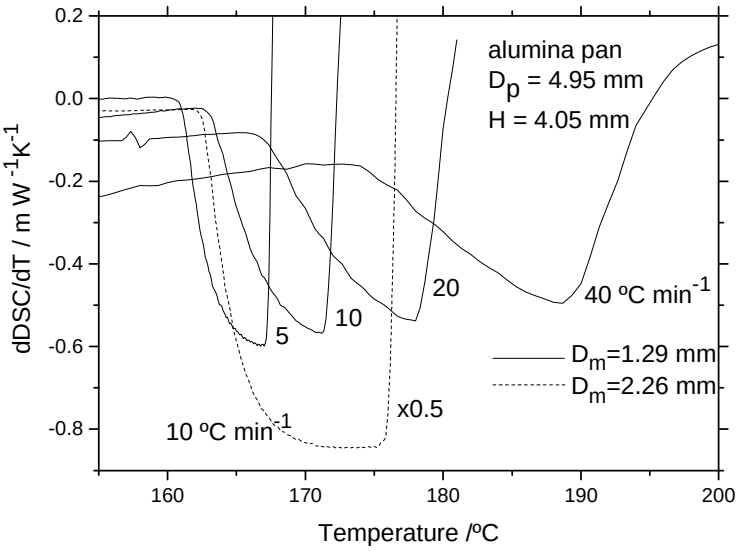

Figure 6.- Slope of the DSC melting peaks for the experiments in Fig.5. Notice that for the smallest metal bead, a constant slope has not been reached.

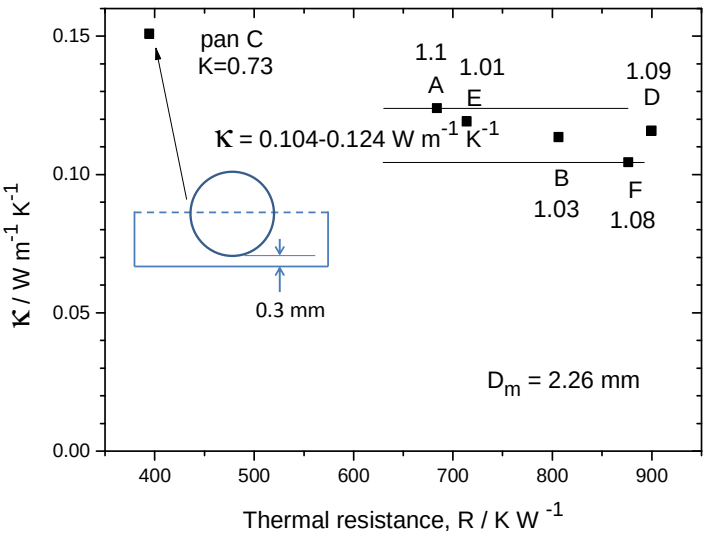

Figure 7.- Thermal conductivity of alumina powders measured with different crucibles and the same In reference bead (D_m = 2.26 mm).

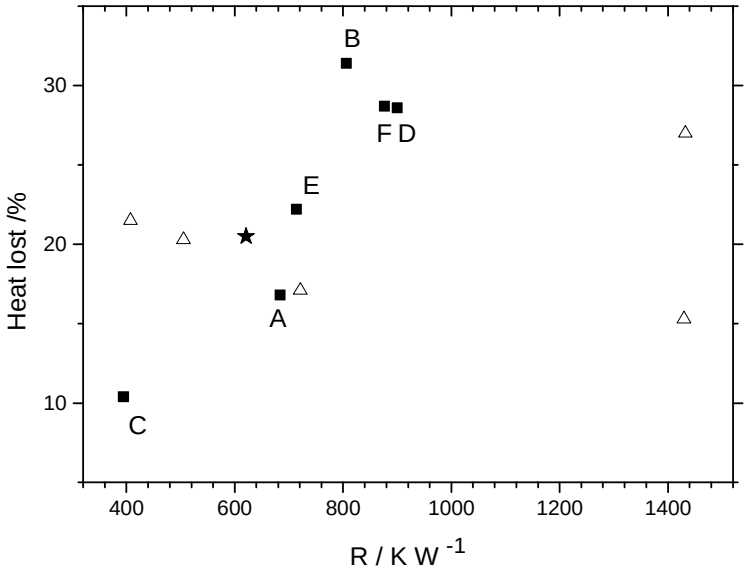

Figure 8.- Heat lost (amount of heat of fusion that is not measured by the DSC sensor) as a function of the powder thermal resistance. Open triangles and full squares correspond to the first and third series of experiments, respectively. Star: hemispherical pan.